International Journal of Mechanical, Industrial and Aerospace Sciences
ISSN: 2517-9950
Vol:12, No:5, 2018

Accuracy of Autonomy Navigation of Unmanned Aircraft Systems through Imagery

Sidney A. Lima, Hermann J. H. Kux, Elcio H. Shiguemori

***Abstract*—**The Unmanned Aircraft Systems (UAS) usually navigate through the Global Navigation Satellite System (GNSS) associated with an Inertial Navigation System (INS). However, GNSS can have its accuracy degraded at any time or even turn off the signal of GNSS. In addition, there is the possibility of malicious interferences, known as jamming. Therefore, the image navigation system can solve the autonomy problem, because if the GNSS is disabled or degraded, the image navigation system would continue to provide coordinate information for the INS, allowing the autonomy of the system. This work aims to evaluate the accuracy of the positioning though photogrammetry concepts. The methodology uses orthophotos and Digital Surface Models (DSM) as a reference to represent the object space and photograph obtained during the flight to represent the image space. For the calculation of the coordinates of the perspective center and camera attitudes, it is necessary to know the coordinates of homologous points in the object space (orthophoto coordinates and DSM altitude) and image space (column and line of the photograph). So if it is possible to automatically identify in real time the homologous points the coordinates and attitudes can be calculated whit their respective accuracies. With the methodology applied in this work, it is possible to verify maximum errors in the order of 0.5 m in the positioning and 0.6º in the attitude of the camera, so the navigation through the image can reach values equal to or higher than the GNSS receivers without differential correction. Therefore, navigating through the image is a good alternative to enable autonomous navigation.

***Keywords*—**Autonomy, navigation, security, photogrammetry, remote sensing, spatial resection, UAS.

I. Introduction

CURRENTLY the use of UAS has increased considerably and became indispensable for several applications where human intervention is dull, dirty, and dangerous. For example, monitoring of the coast [1], search and rescue operation [2], border surveillance [3], precision agriculture [4], forest control [5], forest fires [6], topography [7], photogrammetry [8]-[10], among others.

An application that deserves to be highlighted has been the navigation of UAS, or also known as Drones or Remotely Piloted Aircraft System (RPAS), by automatic image processing, i.e. determination of its position exclusively from features in images generated by a sensor on board [11].

S. A. Lima is with the Institute of Advanced Studies (IEAv), São José dos Campos, SP Mailbox 6044 - 12.228-970 Brazil (phone: +55 12 3947-5352; fax: +55 12 3944-1177; e-mail: sidneysal@ieav.cta.br).

H. J. H. Kux is with the National Institute of Space Research (INPE), São José dos Campos, SP Mailbox 515 - 12.227-010 Brazil (phone: +55 12 3208-6462; e-mail: hermann@dsr.inpe.br).

E. H. Shiguemori is with the Institute of Advanced Studies (IEAv), São José dos Campos, SP Mailbox 6044 - 12.228-970 Brazil (phone: +55 12 3947-5356; e-mail: elcio@ieav.cta.br).

For autonomous UAV arrive in a desired location, it must first be known in which position it is. Thus, the information aircraft positioning is important for navigation, because without it is impossible to navigate autonomously [12]. To solve these problems, one approach is the use of georeferenced images of orbital or airborne sensors of the region of interest and compares them with images obtained at the time of flight. By finding points in common in the two images, one can determine the position of the UAS autonomously [13].

For the navigation of a UAS, three-dimensional coordinates and attitude are required, and this information is usually obtained through GNSS and INS. The inertial systems are autonomous and determine their position in space through accelerometers and gyroscopes. However, over time the position and attitude calculation using only the INS becomes inaccurate, because the INS accumulates errors [14].

In addition to the dependence of GNSS, there is still concern about the possibility of electronic attacks on the GNSS signal, known as jamming or spoofing interference. These attacks can cut off the GNSS signal or decrease accuracy, causing the UAS to lose its location information or even simulate the GNSS signal and report wrong coordinate positions, and can even take control of the UAS, for more information [15].

One of the approaches for autonomous navigation is the use of automatic terrain recognition techniques in images obtained by on board sensors [16]. An automatic recognition with orthophoto and DSM can be employed [11]. With this system the RPAS would be able to generate positioning information instead of GNSS systems.

In this case for the determination of the three-dimensional coordinates and the angles of attitude of the UAV, it is necessary to consider estimation errors [17], [18]. Through the equations of collinearity and adjustment by the method of least squares [19], it is possible to calculate the coordinates and the attitude of the UAS and their respective accuracy, indispensable to determine when the coordinates obtained by the images will be used to correct the INS.

The primary objective of this article is to analyze the accuracies of the determination of the coordinate of perspective center and attitude angles of a camera on board of the UAS using the mathematical modeling necessary for the resolution of the collinearity equations. For such, the difference between this calculated coordinate and a reference coordinate coming from the Bundle Block Adjustment (BBA) used to construct the orthophoto and DSM will be analyzed.

II. Theoretical Foundation

A. Collinearity Equations

Projective transformation is a three dimensional transformation. This geometric transformation takes a system from 3D system (Object Space) to 2D system (Image Space) and vice versa. The mathematical model that translates this transformation is called the collinearity equation [18].

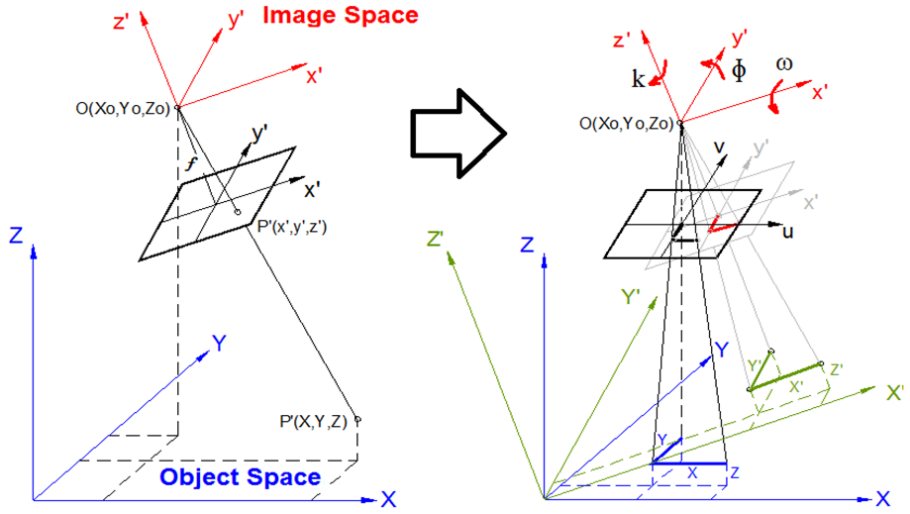

(a) (b)

Fig. 1 Collinearity between Object Space and Image Space

The collinearity equations are based on the concept that the object space, the perspective center (objective of the camera) and the image space are interconnected by a line, as shown in Fig. 1 (a). The photogrammetric coordinate system is defined as follows: the origin coincides with the perspective center; the *Ox* and *Oy* axes are parallel to their homonyms in the fiducial system and oriented in the same way; and the axis Oz is perpendicular to the plane of the negative and forms with the other two a coordinate right-handed system.

Through Fig. 1 (b), the three rotations between a coordinate system in the Image Space and the Object Space are visualized. These rotations are defined by the parameters Omega (ω), Phi (ϕ) e Kappa (k); being respectively the rotations around the *X*, *Y* and *Z* axes [20].

$$M = \begin{bmatrix} \cos\varphi\cos\kappa & \cos\omega\,\mathrm{sen}\,\kappa + \mathrm{sen}\,\omega\,\mathrm{sen}\,\varphi\cos\kappa & \mathrm{sen}\,\omega\,\mathrm{sen}\,\kappa - \cos\omega\,\mathrm{sen}\,\varphi\cos\kappa \\ -\cos\varphi\,\mathrm{sen}\,\kappa & \cos\omega\cos\kappa - \mathrm{sen}\,\omega\,\mathrm{sen}\,\varphi\,\mathrm{sen}\,\kappa & \mathrm{sen}\,\omega\cos\kappa + \cos\omega\,\mathrm{sen}\,\varphi\,\mathrm{sen}\,\kappa \\ \mathrm{sen}\,\varphi & -\mathrm{sen}\,\omega\cos\varphi & \cos\omega\cos\varphi \end{bmatrix} \quad (1)$$

In Fig. 1 (b), four parameters are visualized, namely: a scale factor (f), and three translations (*X-Xo*), (*Y-Yo*) e (*Z-Zo*) between systems. It can be said that this transformation is of the isogonal type, since it has a single scale for the three axes of the two systems. In (2) and (3), we assemble the equations of collinearity that connect the Object Space and Image Space, which are non-linear equations [20].

$$x' = (x - x_0) = -f.\frac{a_{11}(X-X_0)+a_{12}(Y-Y_0)+a_{13}(Z-Z_0)}{a_{31}(X-X_0)+a_{32}(Y-Y_0)+a_{33}(Z-Z_0)} \quad (2)$$

$$y' = (y - y_0) = -f.\frac{a_{21}(X-X_0)+a_{22}(Y-Y_0)+a_{23}(Z-Z_0)}{a_{31}(X-X_0)+a_{32}(Y-Y_0)+a_{33}(Z-Z_0)} \quad (3)$$

where: (x', y') - coordinates in the fiducial system considering the displacement of the principal point; (x, y) - coordinates in the fiducial system; (x_0, y_0) - coordinates of the principal point in fiducial system; (X, Y, Z) - coordinates of the geodetics system; (X_0, Y_0, Z_0) - coordinates of the perspective center in geodetics system; f - Scale between fiducial and geodetics system; e; a_{ij} - Parameters by rotation matrix.

B. Geometric Distortions in Photographic Images

A raw image contains geometric distortions due to the influence of several intrinsic and extrinsic factors on the sensor. Thus, to obtain reliable metric information from images, it is recommended that the sensor be calibrated. The main task in the photogrammetric process is to establish a strict geometric relation between the image and the object, to extract information from object only through the image [18].

The symmetrical radial distortions can be modeled by the even-numbered polynomial equations in the x and y components of the fiducial mark coordinate system. Usually, only the coefficients K_1, K_2, and K_3 are used [17].

$$R = \sqrt{x^2 + y^2} \quad (4)$$

$$\delta tx = p_1.(R^2 + 2.x^2) + 2.p_2.x.y \quad (5)$$

$$\delta ty = p_2.(R^2 + 2.y^2) + 2.p_1.x.y \quad (6)$$

The tangential distortion comes from the manufacturer's inability to perfectly align the optical axes of the lens that compose an objective, resulting in the displacement of the image pixel. These distortions can be modeled using equations in the x and y components of the fiducial mark coordinate system, usually using only the coefficients p_1 and p_2, as shown in (8) and (9) [18].

$$\delta tx = p_1.(R^2 + 2.x^2) + 2.p_2.x.y \quad (7)$$

$$\delta ty = p_2.(R^2 + 2.y^2) + 2.p_1.x.y \quad (8)$$

In order to obtain a mathematical model that best represents the transformation between the object space and image space, it is necessary add to the collinearity equations presented in (2) and (3) the respective radial distortions (δrx, δry) and tangents (δtx, δty) in each component, presented in (5)- (8). Besides the distortions, the coordinates of the principal point (x_0, y_0) must also be considered, and the scale is represented by the focal length of the camera (f), as shown in (9) and (10).

$$x = x_0 + \delta rx + \delta tx - f.\frac{a_{11}(X-X_0)+a_{12}(Y-Y_0)+a_{13}(Z-Z_0)}{a_{31}(X-X_0)+a_{32}(Y-Y_0)+a_{33}(Z-Z_0)} \quad (9)$$

$$y = y_0 + \delta ry + \delta ty - f.\frac{a_{21}(X-X_0)+a_{22}(Y-Y_0)+a_{23}(Z-Z_0)}{a_{31}(X-X_0)+a_{32}(Y-Y_0)+a_{33}(Z-Z_0)} \quad (10)$$

C. Solving Systems of Nonlinear Equations

The resolution of the systems of nonlinear equations is used to calculate the transformation parameters of the collinearity equations, knowing only coordinate of homologous points in the object and image space [17].

For the calculation of the coordinates and attitudes of the perspective center of the camera, at least three points are necessary, when the number of equations is greater than the number of unknowns, which in this case is greater than four points; we have a possible and indeterminate equations system. To solve this type of equations system and estimated the error, the Least Squares Method (LSM) is used. It can be solved by the matrix method, according to (11)-(13) [19].

$$\Delta X = (J^T.P.J)^{-1}.J^T.P.(L - L_0) \quad (11)$$

$$\overline{X} = X_0 + \Delta X \quad (12)$$

$$\Sigma\overline{X} = |\overline{\sigma}|.(J^T.P.J)^{-1} \quad (13)$$

where: ΔX - vector of approximations, that sum to the initial value approximate the value of the unknowns; J - Jacobian Matrix; L - vector of the values observed in the image space; L_0 - vector of the values calculated with the initial parameters, from the object space; P - matrix of the weights of observations; X_0 - vector of the approximate values of the unknowns; $\overline{X}$ - vector of the adjusted unknowns; $\Sigma\overline{X}$ - variance covariance matrix of the adjusted parameters; $\overline{\sigma}$ - variance of the unit of a posteriori weight.

III. Methodology

The methodology used for the analyses of accuracy of the autonomy navigation by image followed the steps is presented in Fig. 2.

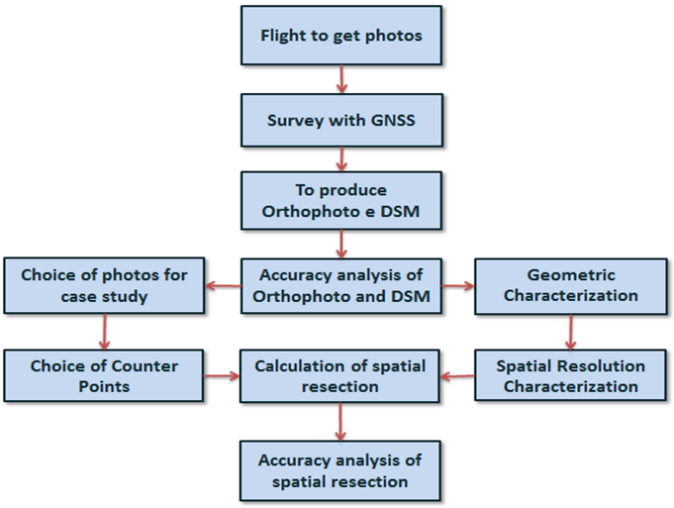

Fig. 2 Methodology workflow

In order to obtain the coordinates of any point in the object space, the aero photogrammetric surveys were carried out to obtain the orthophotos and DSM. In order to know the accuracy of orthophotos and DSM, 15 Ground Control Point (GCP) and 47 Checkpoint were materialized in the field.

In order to test the intrinsic parameters of the camera, which cause distortions in the images, the camera was geometrically characterized and to know the smallest identifiable details the characterization of the spatial resolution was performed.

To test if the position and pointing of the camera influence

the accuracy of the spatial resection, two case studies were chosen: the first with photographs obtained in Nadir's direction and the second in Off Nadir directions.

A. Overflown Area

The experiments were conducted in area located in São José dos Campos, SP, Brazil. The area is close to the São José dos Campos Airport, the flights were coordinated with the Regional Flight Protection Service (SRPV) and Control Tower (TWR) of the São José dos Campos Aerodrome [21].

B. Equipment

The UAS used was a DJI Phantom 4 quadcopter that is able to work autonomously. The GNSS receivers used for survey were the GTR-G2 model from TechGEO with frequencies capability L1 and L2 both GPS and GLONASS constellations. The position of GCP and Checkpoint can be seen in Fig. 3 (a).

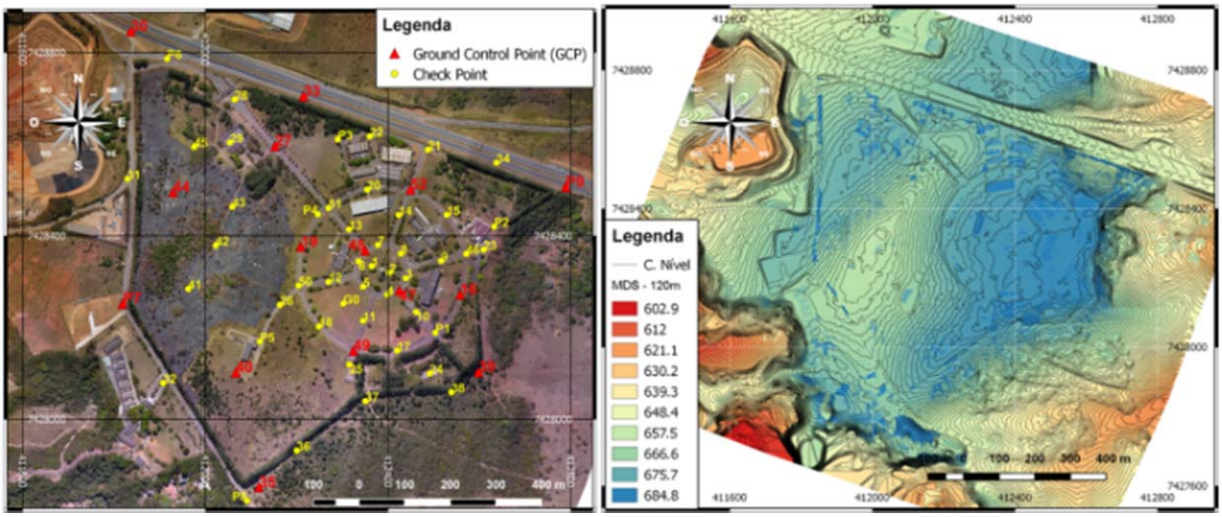

(a) (b)

Fig. 3 (a) Orthophoto and (b) Digital Surface Model (DSM)

C. Data Acquisition and Processing

Flight was planned to cover a 204-hectare area, with 120 m of average height to reach 5.58 cm Ground Sample Distance (GSD), 70% lateral and 75% longitudinal overlap, totalizing 647 photographs.

D. Orthophoto and Digital Surface Model (DSM)

To simulated image navigation, the orthophoto and DSM were used, which were produced in Pix4D Mapper Pro, with 15 Ground Control Point (GCP) and 47 checkpoints.

The statistic of the Mean Sample Error ($\overline{\Delta X}$) and the Standard Deviation Sampling (S) are presented in Table I. The maximum planimetric error observed was 0.567 m, and the minimum error was 0.008 m. Among the 47 checkpoints observed, 61.7% were within the Planimetric Mean Squared Error (DRMS) of 0.321m.

TABLE I
MEAN AND VARIANCE OF THE ORTHOPHOTO AND DSM

Description	E (m)	N (m)	H (m)
Mean Sample Error ($\overline{\Delta X}$)	0.005	-0.017	-0.004
Standard Deviation Sampling (S)	0.252	0.197	0.166
Root Mean Square (RMS)	0.252	0.198	0.166
RMS Planimetric (DRMS)	0.321		

E. Accuracy Analyses of the Space Recession

In order to calculate the spatial resection 30 images at least, with different levels of terrain and different inclinations of the camera were selected and six points were identified in each images, Fig. 4 (a) shows the vertical photograph, and Fig. 4 (b) shows the off Nadir photograph.

(a) (b)

Fig. 4 (a) Nadir photograph and (b) Off Nadir photograph

The images were chosen to verify the error between the coordinate adjusted by the Pix4D and the spatial resection using six control points, being the resolution of the equation system performed by Taylor Series Approximations (TSA) and the calculation of the sample variance by LSM. The software used to solve the collinearity equations and statistical analyzes was Mathcad, according to the methodology presented in [13].

The intrinsic parameters used to calculated the spatial resection were the calibrated focal length (f=3.774 mm); principal point (x_0=3.182 mm, y_0=2.399 mm); radial

distortions coefficients (K_1=-0.007, K_2=0.002, K_3=0.011); tangential distortions coefficients (p_1=0.001, p_2=0.000) and the calibrated sensor size (6.31748 mm, 4.73811 mm).

All of these calibrated data were used to calculate the coordinates and the attitude angles of the perspective center of the camera in space at the time they were taken. After that, these data were compared with the reference coordinate, which comes from the Bundle Block Adjustment (BBA) calculated by Pix4D Mapper Pro to produce the orthophoto and DSM. The result of the deviations can be visualized in the boxplot graphs of Fig. 5.

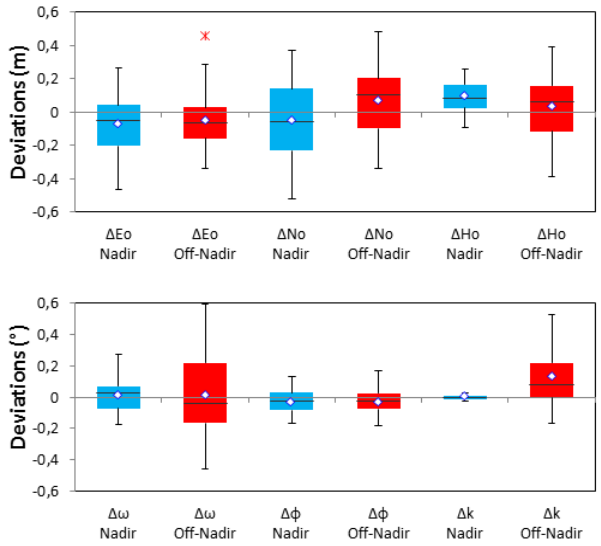

Fig. 5 Boxplot deviation of Perspective Center and Attitude of photos

IV. Conclusion

Based on the results, it can be verified that it is possible to determine, by spatial resection, the coordinates and attitude angles of a camera in space, with their respective variances. Thus, it is possible to navigate using images with accuracy close to GNSS, for this one must configure the image navigation system with characteristics compatible with the accuracy required for the navigation system required for each project. There are several ways of calculating spatial resection, and for the sake of navigation, one should choose the method that is most appropriate for on-board and real-time operation.

Thus, in order to obtain reliable metric information from images in the various applications, it is essential that the sensor be calibrated geometrically. These parameters can improve the accuracy of positioning. Therefore, by integrating the image navigation system with an INS, if GNSS fails, UAS will be able to continue navigating, making the system autonomous.

References

[1] J. A. Gonçalves and R. Henriques, "UAV photogrammetry for topographic monitoring of coastal areas," *ISPRS J. Photogramm. Remote Sens.*, vol. 104, pp. 101–111, 2015.

[2] J. Roberts, D. Frousheger, B. Williams, D. Campbell, and R. Walker, "How the outback challenge was won," *IEEE Robot. Autom. Mag.*, vol. 23, no. 4, pp. 54–62, 2016.

[3] R. O. Andrade, "O voo do falcão." FAPESP, São Paulo, p. v.211, 64-69, 2013.

[4] P. J. Zarco-Tejada, R. Diaz-Varela, V. Angileri, and P. Loudjani, "Tree height quantification using very high resolution imagery acquired from an unmanned aerial vehicle (UAV) and automatic 3D photo-reconstruction methods," *Eur. J. Agron.*, vol. 55, pp. 89–99, 2014.

[5] J. P. Dash, M. S. Watt, G. D. Pearse, M. Heaphy, and H. S. Dungey, "Assessing very high resolution UAV imagery for monitoring forest health during a simulated disease outbreak," *ISPRS J. Photogramm. Remote Sens.*, vol. 131, pp. 1–14, 2017.

[6] H. Sun, G. Song, Z. Wei, Y. Zhang, and S. Liu, "Bilateral teleoperation of an unmanned aerial vehicle for forest fire detection," *2017 IEEE Int. Conf. Inf. Autom. ICIA 2017*, no. July, pp. 586–591, 2017.

[7] M. R. James, S. Robson, S. D'Oleire-Oltmanns, and U. Niethammer, "Optimising UAV topographic surveys processed with structure-from-motion: Ground control quality, quantity and bundle adjustment," *Geomorphology*, vol. 280, pp. 51–66, 2017.

[8] F. C. Nogueira and L. Roberto, "Accuracy analysis of orthomosaic and DSM produced from sensor aboard UAV," *XVIII Simpósio Bras. Sensoriamento Remoto -SBSR*, vol. d, no. 2011, pp. 4880–4887, 2017.

[9] F. Agüera-Vega, F. Carvajal-Ramírez, and P. Martínez-Carricondo, "Assessment of photogrammetric mapping accuracy based on variation ground control points number using unmanned aerial vehicle," *Meas. J. Int. Meas. Confed.*, vol. 98, 2017.

[10] F. Agüera-Vega and F. Carvajal-Ramírez, "Accuracy of Digital Surface Models and Orthophotos Derived from Unmanned Aerial Vehicle Photogrammetry," *J. Surv.*, vol. 143, no. 2, pp. 1–10, 2016.

[11] J. R. G. Braga, H. F. de C. Velho, G. Conte, P. Doherty, and E. H. Shiguemori, "An Image Matching System for Autonomous UAV Navigation Based on Neural Network," *International Conference on Control, Automation, Robotics & Vision (ICARCV)*, Phuket, Thailand, p. 6, 2016.

[12] C. F. Lo *et al.*, "The direct georeferencing application and performance analysis of UAV helicopter in GCP-free area," *ISPRS - Int. Arch. Photogramm. Remote Sens. Spat. Inf. Sci.*, vol. XL-1/W4, no. 1W4, pp. 151–157, Aug. 2015.

[13] S. A. Lima, L. Roberto, E. H. Shiguemori, H. J. H. Kux, and J. L. N. e S. Brito, "Determinação da posição e atitudes de VANT por fotogrametria," *XVIII Simpósio Bras. Sensoriamento Remoto - SBSR*, no. 2008, pp. 5392–5399, 2017.

[14] G. Conte and P. Doherty, "a Visual Navigation System for UAS Based on Geo-Referenced Imagery," *ISPRS - Int. Arch. Photogramm. Remote Sens. Spat. Inf. Sci.*, vol. XXXVIII-1/, no. September, pp. 1–6, 2011.

[15] L. de A. Faria, C. A. de M. Silvestre, and M. A. F. Correia, "GPS-dependent systems: Vulnerabilities to electromagnetic attacks," *J. Aerosp. Technol. Manag.*, vol. 8, no. 4, pp. 423–430, 2016.

[16] P. F. F. Silva Filho, "Automatic Landmark Recognition in Aerial Images for the Autonomous Navigation System of Unmanned Aerial Vehicles," Instituto Tecnológico de Aeronautica - ITA, São José dos Campos, 2016.

[17] P. R. Wolf, B. A. Dewitt, and B. E. Wilkinson, *Elements of Photogrammetry with Applications in GIS*. New York: Mc Graw Hill Education, 2014.

[18] J. C. McGlone and G. Y. G. Lee, *Manual of Photogrammetry*, Sixth. Bethesda, 2013.

[19] C. D. Ghilani, *Adjustament Computations: Spatial Data Analysis*. New Jersey: Wily, 2017.

[20] E. M. Mikhail, J. S. Bethel, and J. C. McGlone, *Introduction to Modern Photogrammetry*. Hobeken: Wiley, 2001.

[21] DECEA/ICA_100-40, *Sistemas de Aeronaves Remotamente Pilotadas e o Acesso ao Espaço Aéreo Brasileiro - ICA 100-40*. Brasil, 2016, p. 56.